

True-amplitude multicomponent migration of elastic wavefields

Alexander Goertz

email: *Goertz@geophysik.fu-berlin.de*

keywords: *imaging, Kirchhoff migration, 3-component seismics, AVO*

ABSTRACT

Kirchhoff depth migration is an imaging process that transforms reflection seismic data into the depth domain in order to obtain a structural image of the subsurface. Mathematically, it can be formulated as a weighted diffraction stack which is related to the Kirchhoff integral representation of the scalar acoustic wave equation and, hence, usually only formulated for imaging of compressional or, more generally, monotypical waves. In this paper, the scalar approach to Kirchhoff imaging based on zero-order ray theory is extended to handle the full elastic wavefield recorded with multicomponent receivers by considering the polarization of respective wave modes scattered at an interface. The weight functions that remove the effect of geometrical spreading from the recorded amplitude change for each scattering mode and have thus to be extended for the case of an elastic multicomponent migration. The extended weight functions presented here are also valid for converted waves. It is shown, that the method allows to retrieve the full elastic scattering matrix of target reflectors.

INTRODUCTION

The graphical migration scheme proposed by Hagedoorn (1954) can be formulated as a summation over the Green's function of the medium. This leads to the so-called Diffraction Stack Integral (DSI) as a wave-equation related integral representation of the graphical image construction technique (Bleistein and Gray, 2001). In the last two decades, several representations of the DSI were developed with slightly different approaches to approximate the (unknown) Green's function of the medium (see, e. g. Bleistein, 1987; Beylkin and Burridge, 1990). These approaches lead to a weighted diffraction stack in which a weight function accounts for the amplitude loss due to geometrical spreading along the propagation path. If other effects on the recorded amplitude can be neglected, this enables the recovery of the angle-dependent reflection coefficient from the migrated image, and is thus called true-amplitude migration.

The approach presented by Schleicher et al. (1993) makes explicit use of zero-order ray theory in order to describe reflections of smoothly-curved first-order discontinuities as the part of the wavefield relevant for imaging. This approach can also be extended to the asymptotically inverse process of demigration, which leads to the so-called unified approach theory to seismic imaging (Hubral et al., 1996; Tygel et al., 1996).

In this paper, the work of the latter three authors, which has so far been strictly formulated only for monotypical reflections (i. e., it did not account for the possibility of mode conversions at an interface) is extended to include the vectorial properties of the elastic wavefield, which can also be described by zero-order ray-theory (Červený, 2001). This approach can then also handle mode-converted reflections.

RAY-THEORETICAL DESCRIPTION OF ELASTIC AMPLITUDES

The correct treatment of the vectorial properties of an elastic wave within the framework of zero-order ray theory requires a formulation of the problem in ray-centered coordinates. Assuming that the elastic wavefield has been recorded in three Cartesian components on a (for simplicity) planar measurement surface, I

can obtain the principle components in ray-centered coordinates by means of a rotation (Červený, 2001):

$$\vec{U}(\vec{\xi}, t) = \begin{pmatrix} U_{SV} \\ U_{SH} \\ U_P \end{pmatrix} = \mathbf{H}^T \begin{pmatrix} U_x \\ U_y \\ U_z \end{pmatrix}. \quad (1)$$

\mathbf{H} denotes the local rotation matrix from the ray-centered coordinate system to the Cartesian measurement coordinate system. The amplitude $\vec{U}(\vec{\xi}, t)$ stands for the displacement field and subscript P refers to an incoming P-wave that is polarized perpendicular to the wavefront¹ and SV and SH refer to the two principal S wave components within the local tangent plane to the wavefront. The correct rotation of the recorded seismograms into the ray-centered coordinate system will thus enable a separation of the wavefield into its constituting wave modes. The rotation itself requires the knowledge of the local emergence angle of a wavefront; a property which is, as we shall see, also necessary for the calculation of the weight function.

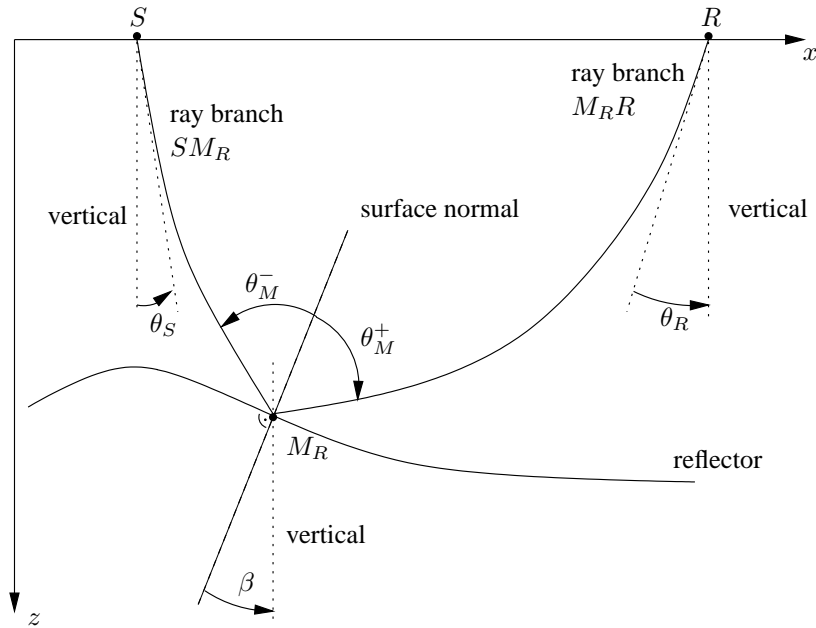


Figure 1: Sketch to explain the geometry of any seismic reflection experiment. Generally, waves are considered that can be described by rays that travel from a source point S at the measurement surface to a depth point M where they are (specularly) reflected by an interface and travel back to a receiver point R at the surface where they are recorded over an aperture A which is densely covered with sources and receivers. The depicted emergence angles are needed for the calculation of the elastic weight function. Note, that for the case of a converted wave, the angles θ_M^- and θ_M^+ are not equal.

I assume that the recorded displacement amplitude has originated from a point source, was reflected by a first-order discontinuity and may have transmitted a number of other reflectors in the overburden, see Figure 1. It can be described by means of the continuation relation (Červený, 2001) as

$$\vec{U}(R) = \frac{1}{v_R v_S \sqrt{\rho_R \rho_S}} \frac{1}{\hat{\mathcal{L}}_{SR}} \left(\prod_{k=1}^{N-1} \hat{\mathbf{T}}_k \right) \hat{\mathbf{R}} \vec{G}(S) e^{i\frac{\pi}{2}\kappa}, \quad (2)$$

with subscript S and R denoting properties at the source and receiver, respectively. $\hat{\mathcal{L}}_{SR}$ denotes the normalized point-source geometrical spreading that can be calculated from the ray Jacobian J as $\hat{\mathcal{L}}_{SR} = \sqrt{\frac{J}{v_r v_s}}$. With this definition (which is due to Schleicher et al., 2002), the geometrical spreading becomes

¹I will restrict myself to the isotropic case

reciprocal². In the following, all reciprocal properties are denoted by a hat. κ denotes the KMAH-index which allows a proper description of the ray Jacobian through caustics. $\prod_{k=1}^{N-1} \hat{\mathbf{T}}_k$ denotes the accumulated effect of transmission loss through the overburden, usually called total transmission loss \mathcal{A} . $\hat{\mathbf{R}}$ is a (3×3) matrix of wave-mode specific reflection/conversion coefficients at the target reflector. It is obtained by satisfying the boundary conditions across the interface, which lead to the well-known Zoeppritz equations (Zoeppritz, 1919). If the local ray-centered tripod is chosen in such a way that the SH component is aligned parallel to the reflecting interface, these boundary conditions simplify, and one obtains a symmetric matrix of reflection coefficients with 5 non-zero components. This results in the fact, that P-waves can only convert in SV -waves and vice versa, whereas SH -waves cannot convert into a different propagation mode. Consequently, I will obtain separate migration formulas for $P - SV$ systems and SH -systems.

Finally, the factor $\vec{G}(S)$ in equation (2) refers to a source term. It contains the source strength and the radiation pattern of the seismic source. In case a P wave is generated at S , the source is omnidirectional and thus $\vec{G} = (0, 0, f_0)^T$ with f_0 being the source strength. This would be the representation of an explosive source. For an S wave generated at the source, \vec{G} can be much more complex. For the most general case, it is represented by means of the Seismic Moment Tensor \mathbf{M}_0 which expresses the source directivity in terms of nine elementary force couples (see, e.g., Aki and Richards, 1980). For the purpose followed in this paper, a moment tensor point source can be written in a high-frequency asymptotic sense according to Červený et al. (1987) as

$$\vec{G}(S) = \frac{1}{4\pi\rho_s v_s} \mathbf{H}^T \mathbf{M}_0 \vec{p}_0, \quad (3)$$

where \vec{p}_0 denotes the initial slowness vector at the source. Since \mathbf{M}_0 and \vec{p}_0 are expressed in a Cartesian coordinate system at the source, the rotation matrix \mathbf{H} introduced in equation (1) has to be employed again to obtain an expression for \vec{G} in ray-centered coordinates.

Definition of elastic true-amplitude traces

It has to be noted that in reality there exist quite a few more processes that may affect the amplitude of the recorded wavefield. Among these are attenuation effects, receiver array directivity, ground coupling of geophones, just to name a few (Sheriff, 1975). In the following, I assume that all these effects can be either neglected or corrected for. Likewise, the transmission loss \mathcal{A} can be neglected as it is usually a slowly varying quantity compared to the amplitude variation with offset (AVO) behavior. It could be corrected for by a layer-stripping approach. As a summary, one can approximate the elementary reflection in equation (2) in terms of a transient solution within the framework of zero-order ray theory as

$$\vec{U}(R(\vec{\xi}), t) \approx \frac{1}{v_R v_S \sqrt{\rho_R \rho_S}} \frac{\hat{\mathbf{R}}}{\hat{\mathcal{L}}} \vec{G}^0 F[t - \tau_R(\vec{\xi})], \quad (4)$$

where the source wavelet is specified by an analytic source pulse $F[t]$, shifted to the arrival time τ_R which denotes the reflection traveltime along the ray $S(\vec{\xi})M_R R(\vec{\xi})$ (see Figure 1). \vec{G}^0 denotes the source directivity function normalized by the source strength.

A true-amplitude process aims at recovering the reflection coefficient $\hat{\mathbf{R}}$ from a seismic trace. Since the reflection coefficient consists of five non-zero components (four for $P - SV$ systems and one for SH systems), we are able to define true-amplitude traces in a system of five equations by interchanging the applicable components of each term in equation (4) for each ray code. Each true-amplitude trace consists of the seismic source signal (at the correct reflection time for the specified ray code) multiplied only by the respective component of the reflection Matrix $\hat{\mathbf{R}}$. Consequently, one may write

$$U_{ij}^{TA} = \hat{R}_{ij} F[t - \tau_{ij}(\vec{\xi})] \approx v_{i,S} v_{j,R} \sqrt{\rho_S \rho_R} \frac{\hat{\mathcal{L}}}{G_i^0} U_j(\vec{\xi}, t - \tau_{ij}), \quad (5)$$

²Also, defined in this manner, $\hat{\mathcal{L}}$ equals the length of the ray between S and R for homogeneous media, which is according to our physical intuition.

where the index i denotes either P , SV , or SH on the source side and index j likewise the respective component on the receiver side:

$$i, j = \begin{cases} P, SV & \text{for } P - SV \text{ systems} \\ i = j = SH & \text{for } SH \text{ systems.} \end{cases} \quad (6)$$

Subscripts S and R in equation (5) refer now and in the following to properties at the source and receiver, respectively, and τ_{ij} refers to the reflection traveltime of the specified ray code. G_i^0 denotes the component of the source directivity function and U_j stands for the respective component (in ray-centered coordinates) of the recorded signal.

The true-amplitude migration introduced in the following section will perform exactly this operation, i.e., applying a weight piecewise to the data and interchanging the relevant properties and components for each ray code in such a way, that the resulting amplitude equals the respective reflection/conversion coefficients at the migrated interface. This means also, that the migrated image will consist in the most general case of five components for each of the five components of the reflectivity matrix.

TRUE-AMPLITUDE DIFFRACTION STACK

Mathematically, the Kirchhoff migration process is expressed as an integration over the recorded wavefield and reads for scalar wavefields in 3-D (Tygel et al., 1996)

$$V(M) = -\frac{1}{2\pi} \iint_A d\xi_1 d\xi_2 W_{DS}(\vec{\xi}, M) \left. \frac{\partial U(\vec{\xi}, t)}{\partial t} \right|_{t=\tau_D(\vec{\xi}, M)}. \quad (7)$$

$V(M)$ is the value assigned to one diffraction point M in the depth domain after migration and $U(\vec{\xi}, t)$ denotes the (scalar) data in the time domain. These data are assumed to consist of analytic traces, i. e., the actual trace recorded in the field as the real part and its Hilbert transform as the imaginary part. Sources and receivers are grouped into pairs, whose locations are described as a function of $\vec{\xi}$. The actual form of this function depends on the measurement configuration. The migration aperture A is the area over which $\vec{\xi}$ varies to cover all source-receiver pairs used in the stack. The factor $W_{DS}(\vec{\xi}, M)$ is the true-amplitude weight function which removes the effect of geometrical spreading from the migrated amplitude. The stacking surface $\tau_D(\vec{\xi}, M)$ denotes the diffraction traveltime for point M (hence the name diffraction stack) and is called Huygens surface. The time derivative is needed in order to correctly recover the source pulse (Newman, 1975).

For the purpose followed in this paper, I assume an elastic wavefield recorded with an array of three-component receivers. Furthermore, I require that at least one reflection event is present in the seismic data $\vec{U}(\vec{\xi}, t)$. A seismic trace with several (primary) events may be described by superposition of individual seismic events of the type of equation (4). Thus, by applying a Fourier transform to the integral of equation (7) and by inserting the ray-theoretical definition of a true-amplitude trace (5), I obtain a system of equations in the frequency domain

$$\tilde{V}_{ij}(M, \omega) = -\frac{i\omega}{2\pi} \tilde{F}(\omega) \iint_A d\xi_1 d\xi_2 \frac{W_i(\vec{\xi}, M)}{v_{i,S} v_{j,R} \sqrt{\rho_S \rho_R} \hat{\mathcal{L}}} \hat{R}_{ij} G_i^0 e^{i\omega \tau_{dif,ij}}, \quad (8)$$

where the indices i and j are to be permuted as in equation (6). $\tilde{F}(\omega)$ and $\tilde{V}_{ij}(M, \omega)$ denote the Fourier transforms of $F(t)$ and $V_{ij}(M, t)$, respectively. The Migration result $V_{ij}(M)$ is obtained from $\tilde{V}_{ij}(M, \omega)$ by an inverse Fourier transform together with the imaging condition $t = 0$. The term $\tau_{dif,ij}(\vec{\xi}, M)$ is the difference between the diffraction and reflection traveltime for the specified ray code, $\tau_D - \tau_R$.

As is well known, integrals of the above type can be solved by means of the method of stationary phase (see, e. g. Bleistein, 1984). An expression for the weight function is obtained by (a) expanding the phase function $\tau_{dif,ij}$ into a Taylor series up to the second order at the stationary point and (b) comparing the result of the method of stationary phase with the definition of a true-amplitude trace (5). The resulting expression will be a function of the difference between diffraction and reflection traveltime $\tau_{dif,ij}$.

ELASTIC WEIGHT FUNCTION

In the following, I will quickly review how an expression of the weight function can be obtained that consists of the measurable properties along the ray depicted in Figure 1 as well as derivatives of the diffraction traveltime τ_D . This calculation involves mainly the following steps (a more complete compilation of the matter that has been published in the references cited below can be found in Goertz, 2002):

- The geometrical spreading along the ray $SM_R R$ can be decomposed into contributions from the source branch SM_R and the receiver branch $M_R R$ (Hubral et al., 1992a,b).
- Traveltime derivatives can be expressed by means of the so-called Beylkin determinant h_B (Beylkin, 1985; Bleistein, 1987) which consists entirely of derivatives of the diffraction traveltime τ_D and is thus obtainable without the knowledge of a stationary point ξ^* .
- The pulse stretch factor (Tygel et al., 1994) has to be recasted in a more general form that takes into account the fact that the incidence and emergence angles θ_M^- and θ_M^+ at the depth point M are not equal for converted waves (see Figure 1),

$$m_D(\xi^*, M_R) = \left. \frac{\partial \tau_D(\xi^*, M_R)}{\partial z} \right|_{z=\xi^*} = \cos \beta \left(\frac{\cos \theta_M^+}{v_M^+} + \frac{\cos \theta_M^-}{v_M^-} \right). \quad (9)$$

Superscript $-$ denotes properties before and superscript $+$ refers to properties right after reflection or conversion from an interface. For monotypical reflections, $\theta_M^- = \theta_M^+ = \theta_M$ as well as $v_M^- = v_M^+ = v_M$, and thus m_D reduces to the formula published in Tygel et al. (1994).

By consequently considering the difference between incidence and emergence angles in the above outlined points, I obtain the following expression for the weight function:

$$W_i(\vec{\xi}^*, M) = v_{i,S} v_{j,R} \sqrt{\rho_S \rho_R} \mathcal{O}_C \frac{h_B \hat{\mathcal{L}}_{SM} \hat{\mathcal{L}}_{MR}}{G_i^0} e^{i \frac{\pi}{2} (\kappa_S + \kappa_R)}, \quad (10)$$

where the factors κ_S and κ_R denote the KMAH-indices of the ray branches SM and MR . The individual weight function for each ray code is obtained by permutation of the indices i and j for each of the two ray branches according to equation (6). Furthermore, I have introduced a new factor \mathcal{O}_C in equation (10) which reads

$$\mathcal{O}_C = \sqrt{\frac{v_M^+ v_M^-}{\cos \theta_M^+ \cos \theta_M^-}} \left(\frac{\cos \theta_M^+}{v_M^+} + \frac{\cos \theta_M^-}{v_M^-} \right)^{-1}. \quad (11)$$

For the case of monotypical reflections, $\cos \theta_M^+ = \cos \theta_M^- = \cos \theta_M$ and $v_M^+ = v_M^- = v_M$. Thus, if the factor $v_{i,S} v_{j,R} \sqrt{\rho_S \rho_R}$ and the normalized source directivity function G_i^0 are neglected, equation (10) reduces to the well-known formula of Jaramillo et al. (1998)

$$W_{DS}(\vec{\xi}^*, M) = \frac{v_M^2}{2 \cos^2 \theta_M} h_B \hat{\mathcal{L}}_{SM} \hat{\mathcal{L}}_{MR}. \quad (12)$$

Equation (10) represents thus a generalization of the weight function for the case of mode-converted reflections. Note that the factor $v_{i,S} v_{j,R} \sqrt{\rho_S \rho_R}$ changes for different propagation modes and thus cannot be neglected.

The factor \mathcal{O}_C defined in equation (11) can be reformulated in such a way, that it contains the sum of the emergence angles of a diffracted ray at M measured towards the vertical instead of the actual reflection/conversion angles at a point of specular reflection M_R . It then reads

$$\mathcal{O}_C = v_M^+ v_M^- \sqrt{\frac{v_M^- v_M^+}{(v_M^+ + v_M^- \cos(\alpha_M^S + \alpha_M^R))(v_M^- + v_M^+ \cos(\alpha_M^S + \alpha_M^R))}}, \quad (13)$$

where α_M^S and α_M^R denote the angles the source and receiver segments make with the vertical axis at the depth point M . These angles are independent of the reflector dip angle β . The derivation of equation (13)

can be found in Appendix A.

Equation (13) expresses the important fact, that the weight function of equation (10) is independent of any reflector properties at point M . The velocities v_M^+ and v_M^- are known from the (elastic) macro-velocity model. The angle $(\alpha_M^S + \alpha_M^R)$ can be calculated for any diffracted ray in the subsurface at any point M , irrespective of whether it is an actual reflection point M_R or not. The geometrical spreading factors of the two ray branches SM and MR can be determined by means of dynamic ray tracing. Finally, the Beylkin determinant consists, as mentioned, only of derivatives of the diffraction traveltime τ_D . This means that, although all the derivations so far were made under the assumption of an actual reflection point M_R , equation (10) is generally valid for *any* depth point M in the macro-velocity model.

Let me finally mention, that the approach presented by Schleicher et al. (1993) results in a weight function that does not involve the Beylkin determinant. Rather, h_B can be further decomposed (Schleicher et al., 2002)

$$h_B = \frac{m_D}{\cos \beta} |\det(\Gamma_S \mathbf{N}_{SM} + \Gamma_R \mathbf{N}_{MR})|, \quad (14)$$

where Γ_S and Γ_R are (2×2) configuration matrices describing the source and receiver positions with respect to the chosen measurement configuration. They are either the zero matrix \mathbf{O} or the identity matrix \mathbf{I} . For the case of, e.g., a common-shot experiment, the source position does not vary, thus $\Gamma_S = \mathbf{O}$ and $\Gamma_R = \mathbf{I}$. For a common-offset experiment (which is mainly considered in the following), both matrices Γ_S and Γ_R are unity, i.e., the identity matrix. The Matrices \mathbf{N}_{SM} and \mathbf{N}_{MR} are second-order mixed-derivative Hessian matrices of traveltimes with respect to the positions of the source and receiver. These matrices relate to the geometrical spreading (Hubral et al., 1992a) as

$$\hat{\mathcal{L}}_{SM} = \sqrt{\frac{\cos \theta_S \cos \theta_M^-}{v_S v_M^-}} (\det \mathbf{N}_{SM})^{-\frac{1}{2}} e^{-i\frac{\pi}{2} \kappa_{SM}}, \quad (15)$$

$$\hat{\mathcal{L}}_{MR} = \sqrt{\frac{\cos \theta_R \cos \theta_M^+}{v_R v_M^+}} (\det \mathbf{N}_{MR})^{-\frac{1}{2}} e^{-i\frac{\pi}{2} \kappa_{MR}}. \quad (16)$$

Upon insertion of relation (15) and (14) into the weight function of equation 10, I obtain an expression of the weight function which depends only on (mixed) traveltime derivatives and the properties at the measurement surface

$$W_i(\vec{\xi}^*, M) = \frac{\sqrt{v_{i,S} v_{j,R} \rho_S \rho_R \cos \theta_S \cos \theta_R}}{G_i^0} \frac{|\det(\Gamma_S \mathbf{N}_{SM} + \Gamma_R \mathbf{N}_{MR})|}{\sqrt{\det \mathbf{N}_{SM}} \sqrt{\det \mathbf{N}_{MR}}} e^{-i\frac{\pi}{2}(\kappa_S + \kappa_R)}, \quad (17)$$

which can be considered as a generalization of the weight function derived by Schleicher (1993). The only difference, however, are the forefactors under the square root and the source term G_i^0 which cannot be neglected for the case of mode-converted waves.

Special cases

One of the advantages of equation (17) is the fact that can be easily simplified for some special cases of the measurement configuration. For the case of a common-shot or a common-receiver configuration, the sum in the determinant of equation (14) vanishes since one of the configuration matrices Γ becomes zero. For these cases, the numerator of equation (17) simplifies, and by employing equation (15) again, I obtain

$$W_{ij,CS} = \sqrt{\rho_{S,i} \rho_{R,j}} v_{S,i} \cos \theta_{R,j} \mathcal{O}_G \frac{\hat{\mathcal{L}}_{SM}}{\hat{\mathcal{L}}_{MR}} \frac{1}{G_i^0} \quad \text{for common shot}, \quad (18)$$

$$W_{ij,CR} = \sqrt{\rho_{S,i} \rho_{R,j}} v_{R,j} \cos \theta_{S,i} \frac{1}{\mathcal{O}_G} \frac{\hat{\mathcal{L}}_{MR}}{\hat{\mathcal{L}}_{SM}} \frac{1}{G_i^0} \quad \text{for common receiver} \quad (19)$$

configurations. Here, the factor \mathcal{O}_G contains the incidence and reflection angle at the depth point M which can be formulated in terms of the diffraction angles measured towards the vertical according to equation

(35):

$$\mathcal{O}_G = \sqrt{\frac{v_M^- \cos \theta_M^+}{v_M^+ \cos \theta_M^-}} \stackrel{(35)}{=} \sqrt{\frac{(v_M^-)^2 + v_M^- v_M^+ \cos(\alpha_M^S + \alpha_M^R)}{(v_M^+)^2 + v_M^- v_M^+ \cos(\alpha_M^S + \alpha_M^R)}}. \quad (20)$$

For the case of monotypical reflections the factor \mathcal{O}_G vanishes, and by neglecting the forefactors again, these weights reduce to the expressions published by Hanitzsch (1997).

Since the final aim of a true-amplitude migration is the extraction of the AVO behavior at a depth point M , the actually desired measurement configuration is a common-offset (CO) geometry. For this measurement configuration, both matrices $\mathbf{\Gamma}$ become the identity matrix and thus, the sum under the determinant in equation (14) remains. Unfortunately, it is in general not possible to interchange a summation with taking the determinant. Mathematically, this is only possible, if at least one row of the two (2×2) matrices to be summed is identical. This is the case for a *laterally homogeneous* medium, i.e., when the velocity is only a function of depth, $v = v(z)$. Then, every ray SMR in a 3-D acquisition geometry is confined to a plane, and the derivatives perpendicular to this plane (and thus one row of the matrices \mathbf{N}) are identical. For this special case only, equation (17) can be simplified by employing again equations (15) and (35)

$$W_{ij,v(z)} = \frac{\sqrt{\rho_{S,i} \rho_{R,j}}}{G_i^0} \left(v_{S,i} \cos \theta_{R,j} \mathcal{O}_G \frac{\hat{L}_{SM}}{\hat{L}_{MR}} + v_{R,j} \cos \theta_{S,i} \frac{1}{\mathcal{O}_G} \frac{\hat{L}_{MR}}{\hat{L}_{SM}} \right), \quad (21)$$

where the factor \mathcal{O}_G is again given by equation (20). The validity of equation (21) for a laterally homogeneous medium only may seem as a strong restriction, but is justifiable in many practical applications. For arbitrary 3-D media, however, the derivatives of either the Matrices \mathbf{N} in equation (17) or the Beylkin determinant in equation (10) have to be calculated directly.

Wavefield separation

All the derivations so far were made under the assumption, that the data in the time domain was acquired in ray-centered coordinates where the P and S wavefields are already separated. This separation of the P and S wavefields can be done independently for each diffracted ray during migration by means of equation (1). The rotation angles are the angle of emergence $\theta_{j,R}$ that occur already in the weight function of equation (17). I can therefore extend the diffraction stack integral of equation (7) for the migration of elastic wavefields as follows:

$$V_{ij}(M) = -\frac{1}{2\pi} \iint_A d\xi_1 d\xi_2 W_i(\vec{\xi}, M) \frac{\partial}{\partial t} \left(H_{jk}(R) U_k(\vec{\xi}(R), t) \right) \Bigg|_{t=\tau_{D,ij}(\vec{\xi}, M)}, \quad (22)$$

where the weight function (or *true-amplitude kernel*) W_i is given by either equation (10) or, alternatively, equation (17). H_{jk} denotes the components of the rotation matrix \mathbf{H}^T introduced in equation (1). U_k then refers to the recorded wavefield in Cartesian coordinates. The components of the rotation matrix consist of direction cosines,

$$U_j(R) = H_{jk}(R) U_k(R) = \frac{\partial q_j}{\partial x_k} U_k \Bigg|_R. \quad (23)$$

For practical use, the rotation into ray-centered coordinates is best performed during migration together with the application of the weight function. Then, the direction cosines of the rotation matrix can easily be combined with the ones of the source directivity function G_i^0 . A table of direction cosines combined in this manner can be found in Traub (1999) for the most commonly used P and S wave sources. These direction cosines contain not only the angle of emergence θ_R towards the vertical at the receiver (see Figure 1), but also the azimuth ϕ_R , i.e., the emergence angle within the (horizontal) measurement plane.

ELASTIC MIGRATION IN 2.5-D

In 2.5-D, i.e., when the medium does not vary with respect to the coordinate perpendicular to the seismic line (crossline direction), the out-of-plane ξ_2 -integration in equation (8) can be evaluated analytically. Since

all data acquired on lines parallel to the actual seismic line would be identical, the migration aperture A can be assumed to be infinite in the ξ_2 -direction. Kirchhoff migration then reduces to an in-plane stack over the aperture interval (a, b) in the ξ_1 -direction covered by the seismic line. Since ξ_1 is now the only integration variable, we can drop the index 1 to write the 2.5-D Kirchhoff migration integral as

$$\tilde{V}_{ij}(M, \omega) = \sqrt{\frac{-i\omega}{2\pi}} \tilde{F}(\omega) \int_a^b d\xi \frac{1}{v_{i,S} v_{j,R} \sqrt{\rho_S \rho_R} \hat{\mathcal{L}}} W_i^{(2.5)}(\xi, M) \hat{R}_{ij} G_i^0 e^{i\omega\tau_{dif,ij}}, \quad (24)$$

where $W_i^{(2.5)}$ is the 2.5-D weight factor that guarantees true amplitudes in this 1-D stack. It is composed of the 3-D weight factor and the result of the analytic solution of the out-of-plane integral. Since in the 2.5-D situation, the target model does not vary in the ξ_2 -direction, it suffices to regard only one S wave component. One may therefore skip the treatment of SH systems and instead restrict the situation to only two components recorded at the surface, a P component and one S component aligned with the acquisition line. However, we still consider a 3-dimensional wave propagation and thus $\hat{\mathcal{L}}$ carries the full 3-D geometrical spreading.

For the derivation of a 2.5-D weight function, the following three points have to be considered:

- The (3-D) geometrical spreading $\hat{\mathcal{L}}$ can be split into an in-plane part $\bar{\mathcal{L}}$ and an out-of-plane part σ , with $\hat{\mathcal{L}} = \bar{\mathcal{L}}\sqrt{\sigma}$.
- According to equation (24), the migration integral reduces to an in-plane stack and the corresponding stacking operators reduce to lines. The out-of-plane integration can be evaluated analytically and yields (Bleistein et al., 1987) a factor $\left(\frac{1}{\sigma_S} + \frac{1}{\sigma_R}\right)^{-\frac{1}{2}}$ which has to be applied additionally to the weight function.
- The Beylkin determinant, and, due to equation (14), also the determinant in the numerator of equation (17) simplify which allows to extract an additional factor $\left(\frac{1}{\sigma_S} + \frac{1}{\sigma_R}\right)$. In the same manner as described above, one may then interchange the summation with taking the determinant which allows to give an expression for a 2.5-D common-offset weight function that does not contain traveltimes derivatives.

The out-of-plane spreading factors σ_S and σ_R are defined by the path integral $\sigma = \int v ds$ with s being the arc length along the rays SM and MR . Altogether, I obtain for the 2.5-D common-offset case

$$W_{ij,2.5D} = \frac{\sqrt{\rho_{S,i}\rho_{R,j}}}{G_i^0} \left(v_{S,i} \cos\theta_{R,j} \mathcal{O}_G \frac{\bar{\mathcal{L}}_{SM}}{\bar{\mathcal{L}}_{MR}} + v_{R,j} \cos\theta_{S,i} \frac{1}{\mathcal{O}_G} \frac{\bar{\mathcal{L}}_{MR}}{\bar{\mathcal{L}}_{SM}} \right) \sqrt{\sigma_S + \sigma_R}, \quad (25)$$

where the factor \mathcal{O}_G is defined in equation (20) and $\bar{\mathcal{L}}$ denotes now the (2-D) in-plane geometrical spreading. For the case of monotypical reflections, the factor \mathcal{O}_G vanishes again, and equation (25) reduces to the formula published by Hanitzsch (1997), if constant factors are neglected again. Weight functions for common-shot and common-receiver configurations can be derived accordingly. These are, however, of less importance since a true-amplitude migration aims at recovering the AVO behavior of target reflectors which implies a common-offset migration of multicoverage data.

Please note, that all the derivations so far were made for a *normalized point-source geometrical spreading* as defined by Schleicher et al. (2002). Many textbooks, however, use different notations for the geometrical spreading (including Červený, 2001). Furthermore, the above formulae for the weight function include the source directivity pattern in the denominator which may become zero for certain source types. The problem can be circumvented in practical implementations through a simple case discrimination.

SIMPLE SYNTHETIC EXAMPLE

In the following, I will show a 2.5-D synthetic data example for a flat horizontal interface in a depth of 1 km. The P-wave velocity was chosen to be 2 km/s above the interface and 2.5 km/s below. The

density of the model was kept constant at 2.0 g/cm^3 and the ratio between P- and S-wave velocity was set to 2. A synthetic multicoverage dataset was shot, assuming a roll-along acquisition with an aperture of 3 km in order to illuminate the target reflector well up to overcritical angles. Sources cover a line from 3.0 km to 7.0 km over the model with a spacing of 20 m and generate both P- and S-waves with (for simplicity) a unidirectional radiation pattern for the S-wave. The dominant frequency of the source signal was chosen at 10 Hz in order to safely exclude aliasing effects for all wave modes. The synthetic dataset

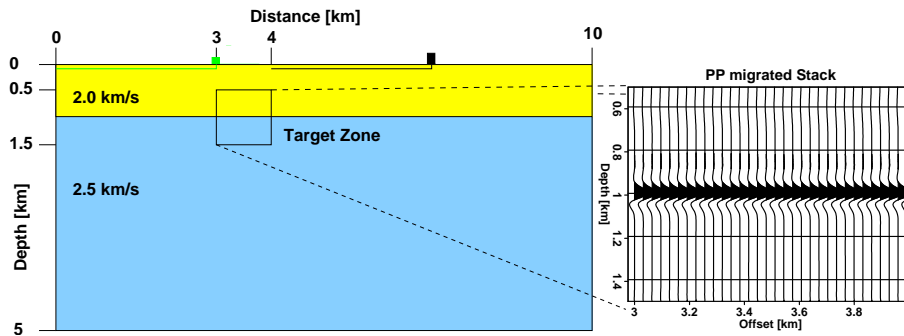


Figure 2: Sketch showing the simple model of a horizontal interface and the chosen acquisition geometry above it. On the right hand side, the prestack depth migration result of the target zone is shown for P to P reflections. Only every second trace is plotted.

consists of 60501 traces that ensure an equal illumination for all offsets for a small target zone between 3.0 km and 4.0 km (see Figure 2). Figure 3 shows one example shot gather for the vertical component (left) and the horizontal component (right). Both seismogram sections show the four principal scattering modes generated at the interface. For this simple case, the $P \rightarrow S$ and $S \rightarrow P$ conversion arrive at the same traveltimes. Nevertheless, the contributions of the two wave modes can clearly be separated by the multicomponent migration.

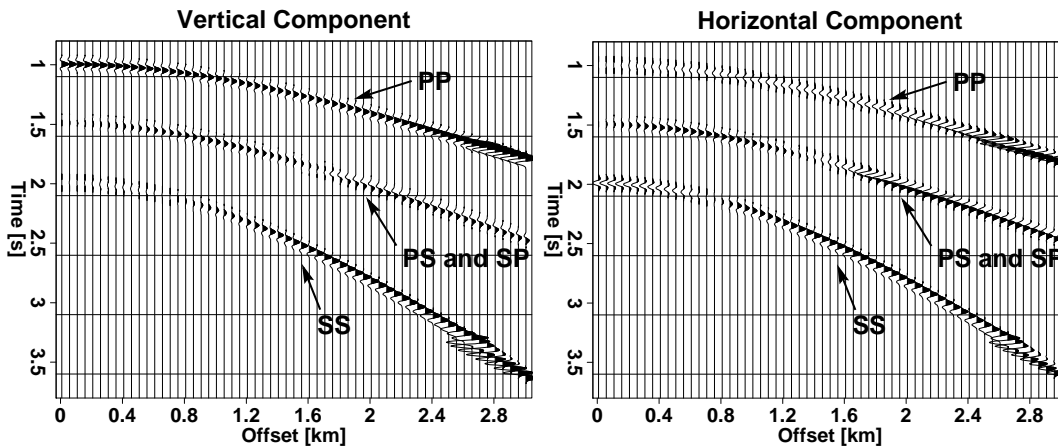


Figure 3: Example shot gather of the vertical (left) and horizontal (right) component of the synthetic multicoverage dataset for a flat layer. Only every 5th trace is shown.

Amplitude evaluation

After a common-offset multicomponent migration employing the weight function of equation (25), one obtains separate migrated images for every offset as well as for every ray code. Figure 4 shows the migrated image gathers for the four principal wave modes contained in the synthetic multicoverage dataset. As can be seen, all four image gathers show a flat event at a depth of 1 km which corresponds to the respective reflection or conversion event from the interface depicted in Figure 2. The reflectivity becomes complex-valued for overcritical angles which results in a phase shift of the migrated signal that is observable at high offsets.

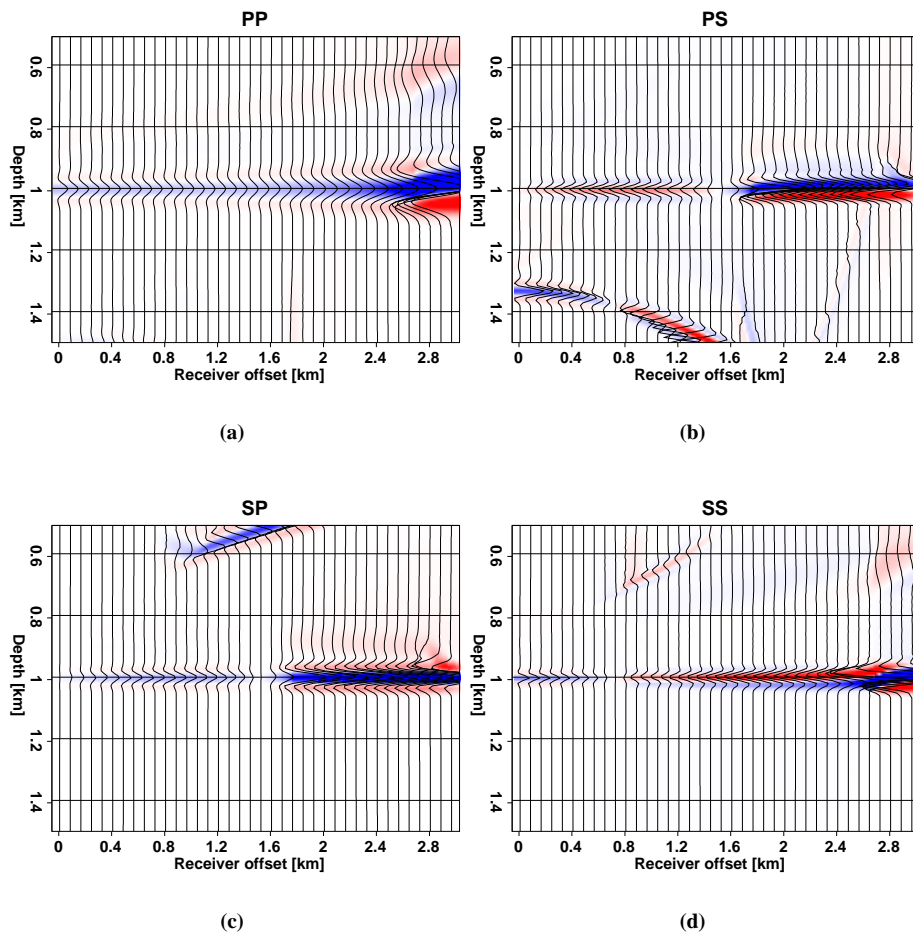


Figure 4: Image gathers of the migration result for the principal wave modes: a) P to P reflection. b) P to S conversion. c) S to P conversion. d) S to S reflection. Blue colors behind the wiggle traces denote positive amplitudes and red colors denote negative amplitudes. Only every 5th trace is shown as wiggle line. Events with moveout stem from other wave modes that appear on the same principal component (see text for discussion).

By picking the amplitudes along the flat events in the image gather, one obtains the desired AVO behavior. If the correct weight function was applied, the picked values should directly yield the reflectivity for the corresponding depth point on a reflector. Figure 5 shows a comparison of the complex magnitudes picked from the migrated image gathers with the theoretically expected values from the Zoeppritz equations for all of the four wave modes. Furthermore, Figure 6 shows a comparison of the phase of the complex reflectivity with the phase shifts picked from the migrated image gathers. As can be seen, both Figure 5

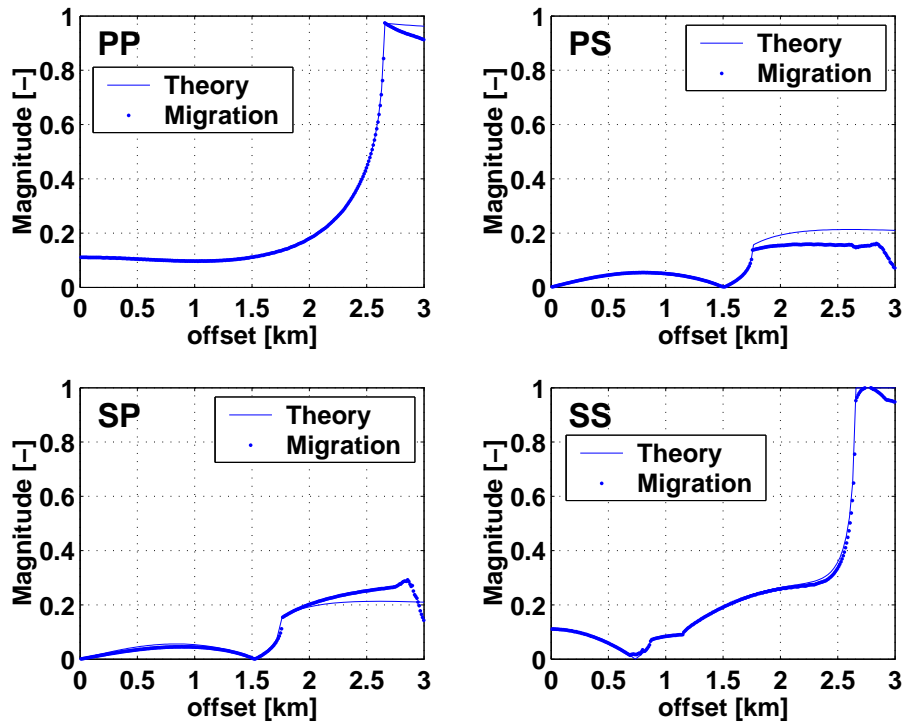


Figure 5: Comparison of amplitudes picked from the migrated image gathers with theoretical values from Zoeppritz equations for every scattering mode: shown are complex magnitudes for P to P (upper left), P to S (upper right), S to P (lower left), and S to S (lower right).

and Figure 6 show a very good agreement of the picked amplitudes with the expected theoretical values. The synthetic time-domain data was generated by using a commercially available wavefront ray tracer that unfortunately proved to calculate the phase of the S to P reflection incorrectly, which explains observable differences in the lower left graph of Figure 6.

Offset stacking

Even after rotation into ray-centered coordinates, the respective input data for one (ray-centered) principal component will contain more than one event since always two modes are arriving at the receiver on the same principal component. In this case, P to P and S to P events will occur on the principal component perpendicular to the wavefront and P to S and S to S events will occur on the principal component tangent to the wavefront. This implies, that the diffraction stack will find stationary points also for events that do not belong to the respective wave mode considered. These events will be mapped incorrectly and thus occur with a considerable moveout in the image gathers. Such events are visible below the $P \rightarrow S$ conversion in Figure 4 (b) and above the $S \rightarrow P$ conversion in Figure 4 (c). These are remnants of the S to S reflection and P to P reflection, respectively. The kinematically correct image for every wave mode is obtained, if all image gathers are stacked in the offset direction. Then, only the correctly migrated (flat) events remain in the final stacked image and all events with moveout in the image gathers will be summed up destructively and thus yield zero.

However, care has to be taken when stacking events with phase changes at overcritical angles (this is the case especially for the conversion modes where the pulse polarity is reversed at high offsets). In order to avoid a destructive summation of such events, one usually stacks the image gathers only for ranges of offsets where phase changes can be neglected. If more than one reflector is present in the data (which is usually the case), these phase changes occur at different offsets for every depth. If furthermore a laterally

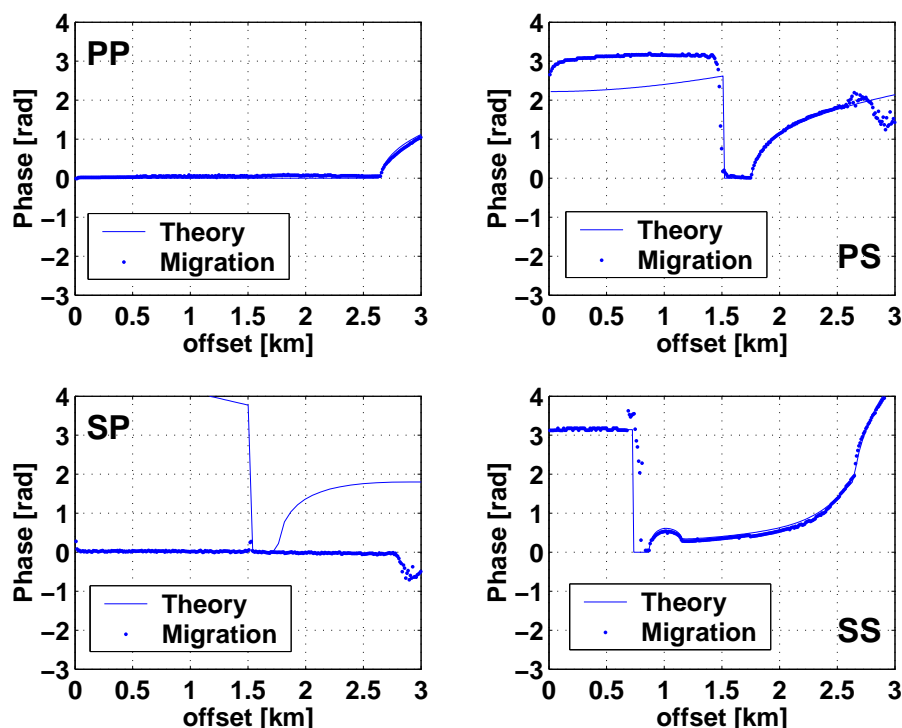


Figure 6: Comparison of the phase of the complex reflectivity picked from the migrated image gathers with theoretical values from Zoeppritz equations for every scattering mode: shown are values for P to P (upper left), P to S (upper right), S to P (lower left), and S to S (lower right).

heterogeneous macro velocity model has to be taken into account, the suitable range for stacking would either have to be chosen individually for every image point (which is impracticable), or the migrated image would have to be sorted according to reflection angle (which implies the knowledge of the reflector dip). In practice, and if the signal-to-noise ratio is sufficiently high, this problem is circumvented by applying several stacks for small ranges of offsets, so-called *near-offset* and *far-offset* stacks.

CONCLUSIONS

The zero-order ray-theory approach to true-amplitude imaging has been restricted so far to the treatment of monotypical reflections, i.e., it did not account for mode conversions at an interface. Here, an extension to this approach is presented that account for the vectorial properties of the elastic wavefield recorded with multicomponent receivers. The resulting weight functions change for every propagation mode and can also be applied to converted waves. Therefore, the procedure allows to retrieve the full matrix of elastic reflection coefficients for all wave modes.

An application of the proposed method to real data requires a uniform and highly controlled coupling of receivers. These requirements may be met for data acquisition within a borehole for vertical seismic profiling (VSP) or on the seafloor for data acquisition with an Ocean Bottom Cable (OBC). The true-amplitude multicomponent imaging method can then have an impact onto amplitude-versus-offset (AVO) inversion which in current applications uses only two parameters: *intercept* (zero-offset reflection coefficient) and *gradient* (near-offset slope of the reflection coefficient) of P to P reflections. If additional information could be retrieved from mode-converted and S-wave reflections, much more parameters can be added to the inversion and less effort needs to be put into calibration with borehole logs from the vicinity.

PUBLICATIONS

Detailed results were published by Goertz (2002).

ACKNOWLEDGMENTS

This work was kindly supported by the Deutsche Forschungsgemeinschaft through grant Ka 1347 and the sponsors of the *Wave Inversion Technology (WIT) Consortium*, Karlsruhe, Germany.

REFERENCES

- Aki, K. and Richards, P. G. (1980). *Quantitative Seismology, vol. 1*. W. H. Freeman & Co., New York.
- Beylkin, G. (1985). Imaging of discontinuities in the inverse scattering problem by inversion of a generalized radon transform. *J. Math. Phys.*, 26:99–108.
- Beylkin, G. and Burridge, R. (1990). Linearized inverse scattering problems in acoustics and elasticity. *Wave Motion*, 12:15–52.
- Bleistein, N. (1984). *Mathematical methods for wave phenomena*. Academic Press Inc., Orlando.
- Bleistein, N. (1987). On the imaging of reflectors in the earth. *Geophysics*, 52(7):931–942.
- Bleistein, N., Cohen, J. K., and Hagin, F. G. (1987). Two and one-half dimensional Born inversion with an arbitrary reference. *Geophysics*, 52(1):26–36.
- Bleistein, N. and Gray, S. (2001). From the Hagedoorn imaging technique to Kirchhoff migration and inversion. *Geophysical Prospecting*, 49(6):629–644.
- Červený, V. (2001). *Seismic Ray Theory*. Cambridge University Press.
- Červený, V., Pleierová, J., Klimeš, L., and Pšenčík, I. (1987). High-frequency radiation from earthquake sources for laterally varying layered structures. *Geophys. J. R. astr. Soc.*, 88:43–79.
- Goertz, A. (2002). *True-amplitude multicomponent migration of elastic wavefields*. PhD thesis, Karlsruhe University.
- Hagedoorn, J. (1954). A process of seismic reflection interpretation. *Geophysical Prospecting*, 2:85–127.
- Hanitzsch, C. (1997). Comparison of weights in prestack amplitude-preserving Kirchhoff depth migration. *Geophysics*, 62(06):1812–1816.
- Hubral, P., Schleicher, J., and Tygel, M. (1992a). Three-dimensional paraxial ray properties – Part I: Basic Relations. *J. Seis. Expl.*, 1:265 – 279.
- Hubral, P., Schleicher, J., and Tygel, M. (1992b). Three-dimensional paraxial ray properties – Part II: Applications. *J. Seis. Expl.*, 1:347 – 362.
- Hubral, P., Schleicher, J., and Tygel, M. (1996). A unified approach to 3-D seismic reflection imaging, part I: Basic concepts. *Geophysics*, 61(3):742–758.
- Jaramillo, H., Schleicher, J., and Tygel, M. (1998). Errata to: A unified approach to 3-D seismic reflection imaging, part II: Theory. *Geophysics*, 63:670–673.
- Newman, P. (1975). Amplitude and phase properties of a digital migration process. In *37th Ann. Internat. Mtg., Europ. Assoc. Expl. Geoph.*, Bergen. (Republished in: *First Break*, 8, 397–403, 1990).
- Schleicher, J. (1993). *Bestimmung von Reflexionskoeffizienten aus Reflexionsseismogrammen*. PhD thesis, Karlsruhe University.
- Schleicher, J., Tygel, M., and Hubral, P. (1993). 3-D true-amplitude finite offset migration. *Geophysics*, 58:1112–1126.

- Schleicher, J., Tygel, M., and Hubral, P. (to appear 2002). *Seismic true-amplitude imaging*. SEG, Tulsa.
- Sheriff, R. (1975). Factors affecting seismic amplitudes. *Geophysical Prospecting*, 23:125 – 138.
- Traub, B. (1999). Seismic Wave Field Modelling in 3D Structures by Means of Recursive Cell Ray Tracing. Master's thesis, Karlsruhe University, Geophysical Institute.
- Tygel, M., Schleicher, J., and Hubral, P. (1994). Pulse distortion in depth migration. *Geophysics*, 59:1561 – 1569.
- Tygel, M., Schleicher, J., and Hubral, P. (1996). A unified approach to 3-D seismic reflection imaging, part II: Theory. *Geophysics*, 61(3):759–775.
- Zoeppritz, K. (1919). Erdbebenwellen VIII b: Über Reflexionen und Durchgang seismischer Wellen durch Unstetigkeitsflächen. *Göttinger Nachrichten*, 1:66–84.

APPENDIX A

In this appendix, I will proof that the factor \mathcal{O}_C introduced in equation (10) is independent of the reflector properties at a point of specular reflection M_R , i.e., it is to proof that

$$\mathcal{O}_C = \sqrt{\frac{v_M^+ v_M^-}{\cos \theta_M^+ \cos \theta_M^-}} \left(\frac{\cos \theta_M^+}{v_M^+} + \frac{\cos \theta_M^-}{v_M^-} \right)^{-1} \quad (26)$$

can be written in such a way that it is independent of the individual angles θ_M^- and θ_M^+ . It will be shown in the following that the factor (26) depends rather on the sum of the angles between the two ray segments (see Figure 7). This sum can be also expressed as the sum of these angles measured towards the vertical which can be calculated for every diffracted ray. As a consequence, the weight function (10) will be generally valid for every subsurface point M , whether or not it is an actual reflection point.

With the use of the trigonometrical addition theorem

$$\cos(\alpha + \beta) = \cos \alpha \cos \beta - \sin \alpha \sin \beta, \quad (27)$$

I may write for the inverse of the second term in in equation (26)

$$\begin{aligned} \frac{\cos \theta_M^+}{v_M^+} + \frac{\cos \theta_M^-}{v_M^-} &= \left(\frac{\cos \theta_M^+}{v_M^+} + \frac{\cos \theta_M^-}{v_M^-} \right) \frac{\cos \theta_M^-}{\cos \theta_M^-} \\ &= \frac{1}{\cos \theta_M^-} \left(\frac{\cos \theta_M^- \cos \theta_M^+}{v_M^+} + \frac{\cos^2 \theta_M^-}{v_M^-} \right) \\ &= \frac{1}{\cos \theta_M^-} \left(\frac{\cos(\theta_M^- + \theta_M^+) + \sin \theta_M^- \sin \theta_M^+}{v_M^+} + \frac{\cos^2 \theta_M^-}{v_M^-} \right). \end{aligned} \quad (28)$$

By using Snell's law for the term $\sin \theta_M^+$,

$$\frac{\sin \theta_M^+}{v_M^+} = \frac{\sin \theta_M^-}{v_M^-} \quad (29)$$

and recalling the fact that $\sin^2 x + \cos^2 x = 1$, I may write for the right hand side of equation (28)

$$\dots = \frac{1}{\cos \theta_M^-} \left(\frac{\cos(\theta_M^+ + \theta_M^-)}{v_M^+} + \frac{1}{v_M^-} \right). \quad (30)$$

By inserting this preliminary result into equation (26), I obtain

$$\begin{aligned} \mathcal{O}_C &= \sqrt{\frac{v_M^+ v_M^-}{\cos \theta_M^+ \cos \theta_M^-}} \left(\frac{\cos \theta_M^- v_M^+ v_M^-}{v_M^- \cos(\theta_M^+ + \theta_M^-) + v_M^+} \right) \\ &= \sqrt{v_M^+ v_M^-} \sqrt{\frac{\cos \theta_M^-}{\cos \theta_M^+}} \left(\frac{v_M^+ v_M^-}{v_M^- \cos(\theta_M^+ + \theta_M^-) + v_M^+} \right). \end{aligned} \quad (31)$$

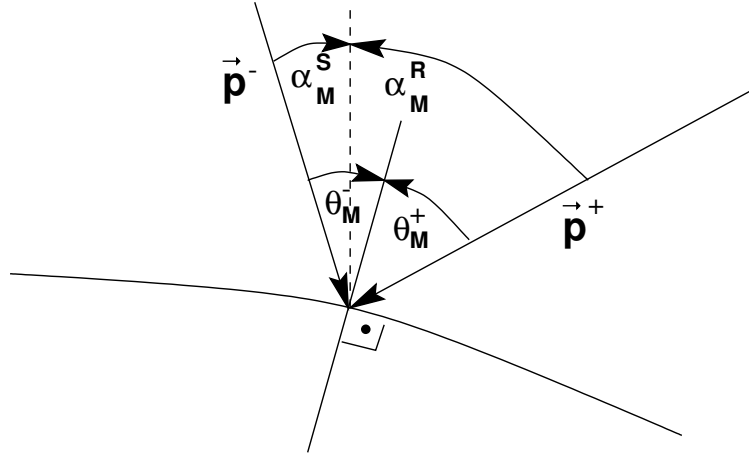


Figure 7: Slowness vectors of a wavefront impinging on an interface.

Now, I turn my attention to the cosines under the square root of equation (31). These can be expressed in terms of the slowness vectors, according to Figure 7 as follows:

$$\cos \theta_M^- = \frac{\vec{p}^- \cdot (\vec{p}^- + \vec{p}^+)}{|\vec{p}^-| |\vec{p}^- + \vec{p}^+|}. \quad (32)$$

The numerator can be calculated by recalling that the length of the slowness vector equals (by definition) the inverse of the velocity, and by expressing its components by means of the angles towards the vertical. Since the two slowness vectors span up a plane, I can confine the calculation to a local (Cartesian) 2-D coordinate system and obtain for the numerator

$$\begin{aligned} \vec{p}^- \cdot (\vec{p}^- + \vec{p}^+) &= (p_x^-)^2 + (p_z^-)^2 + p_x^- p_x^+ + p_z^- p_z^+ = \\ &\stackrel{(27)}{=} \frac{\sin^2 \alpha_M^S}{(v_M^-)^2} + \frac{\cos^2 \alpha_M^S}{(v_M^-)^2} + \frac{\cos(\alpha_M^S + \alpha_M^R)}{v_M^- v_M^+}. \end{aligned} \quad (33)$$

Therefore, I obtain for equation (32) by replacing only $|\vec{p}^-| = \frac{1}{v_M^-}$ in the denominator

$$\cos \theta_M^- = \frac{1}{v_M^- v_M^+} \frac{v_M^+ + v_M^- \cos(\alpha_M^S + \alpha_M^R)}{|\vec{p}^- + \vec{p}^+|}. \quad (34)$$

$\cos \theta_M^+$ can be calculated accordingly and I finally obtain for the ratio of cosines under the square root in equation (31)

$$\sqrt{\frac{\cos \theta_M^-}{\cos \theta_M^+}} = \sqrt{\frac{v_M^+ + v_M^- \cos(\alpha_M^S + \alpha_M^R)}{v_M^- + v_M^+ \cos(\alpha_M^S + \alpha_M^R)}}. \quad (35)$$

From Figure 7, one sees immediately that $\cos(\theta_M^+ + \theta_M^-) = \cos(\alpha_M^S + \alpha_M^R)$ and I thus obtain by inserting equation (35) into equation (31) the final result

$$\mathcal{O}_c = v_M^+ v_M^- \sqrt{\frac{v_M^- v_M^+}{(v_M^+ + v_M^- \cos(\alpha_M^S + \alpha_M^R))(v_M^- + v_M^+ \cos(\alpha_M^S + \alpha_M^R))}}, \quad (36)$$

which is equation (13).